General Disclaimer

One or more of the Following Statements may affect this Document

- This document has been reproduced from the best copy furnished by the organizational source. It is being released in the interest of making available as much information as possible.

- This document may contain data, which exceeds the sheet parameters. It was furnished in this condition by the organizational source and is the best copy available.

- This document may contain tone-on-tone or color graphs, charts and/or pictures, which have been reproduced in black and white.

- This document is paginated as submitted by the original source.

- Portions of this document are not fully legible due to the historical nature of some of the material. However, it is the best reproduction available from the original submission.

NASW-184

SOLAR SATELLITE PROJECT

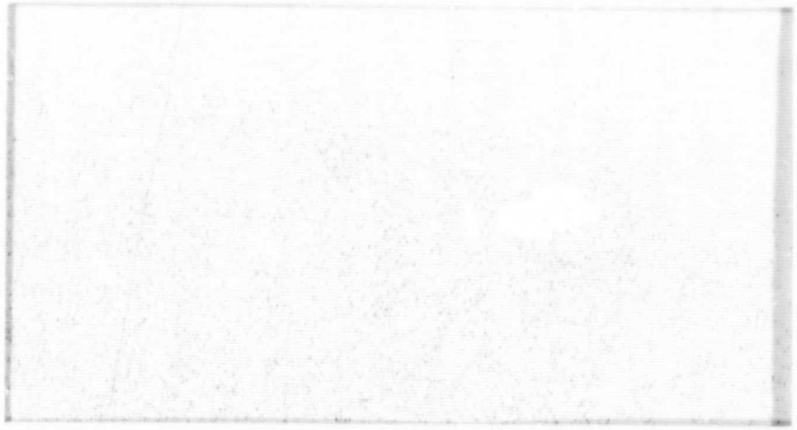

DRF

HARVARD COLLEGE OBSERVATORY

60 GARDEN STREET

CAMBRIDGE, MASS

EXTREME ULTRAVIOLET OBSERVATIONS OF ACTIVE REGIONS IN THE CHROMOSPHERE AND THE CORONA

Technical Report #14

BY

Robert W. Noyes
Smithsonian Astrophysical Observatory
and Harvard College Observatory
Cambridge, Massachusetts

George L. Withbroe and Robert P. Kirshner
Harvard College Observatory
Cambridge, Massachusetts

October 1969

ABSTRACT

New observations of solar active regions have been obtained by the Harvard College Observatory EUV spectroheliometer aboard the OSO-IV spacecraft. From the observations we have determined the enhancement in active regions of the emission from ions formed at various temperatures in the chromosphere and corona. The results are in accord with a simple model of active regions, for which the active region pressure is about five times the quiet sun pressure; the temperature gradient in the transition zone is about five timesthe quiet sun value; and the coronal temperature above active regions is slightly increased.

1. Introduction

Regions of solar activity are practically invisible on the white light solar disk, except for the sunspots which usually accompany them. Their presence is revealed only by the presence of white-light faculae near the limb, which show an enhancement of up to 60 percent relative to nearby quiet areas (Rogerson, 1961).

In the chromosphere and corona, the situation is quite different. The intensity in the Ca^+ K line in active regions is about three times that of the quiet chromosphere (Sheeley, 1967). For O VI, as we shall presently show, the enhancement in active regions is about a factor of eight; for Fe XVI it may exceed 50.

The increased enhancement of intensity in active regions with increased temperature of line formation must reflect the physical structure of active regions. We know, of course, that active regions in the corona are not only denser than their surroundings, as shown by the increased brightness of the white light corona above active regions (Newkirk, 1967); they are also hotter, as is indicated by the increased [Fe XIV]and [Ca XV] emission above them. However, the detailed variation

of density and temperature with height in active regions is not well known. In this paper we present new observations of active-region enhancement of individual ions in the chromosphere and corona, and discuss the implications of these data for the structure of active regions in the upper solar atmosphere.

2. Observations

The Harvard College Observatory ultraviolet spectroheliometer aboard the OSO-IV spacecraft has obtained much new information about the ultraviolet emission from active regions. During October and November 1967 we obtained spectroheliograms in a variety of emission lines from ions with temperatures of formation ranging from 10^4 to 4×10^6 °K. These data permit us for the first time to obtain quantitative knowledge of the enhancement of active region emission in the upper chromosphere and corona.

Since the details of the spectroheliometer are described elsewhere (Goldberg et al., 1968), here we merely summarize its characteristics. Spectroheliograms could be obtained at any wavelength between 300 and 1400Å, with a spatial resolution of one square arcmin, and a spectral resolution

of 3Å (hence the entire emission from the spectral line passed through the entrance slit). About 10 spectroheliograms were obtained at a selected wavelength during the daylight portion of each spacecraft orbit.

In addition, spectra of an area one arcmin square at the center of the solar disk were obtained daily. The spectra covered the range 300 - 1400Å, with a spectral resolution of 3Å. About 30 minutes were required to obtain each scan. Since the center of the disk was close to the quiet equator during the time of operation, the spectra are characteristic of the quiet sun.

Figure 1 shows a sample of the spectroheliograms, plotted in an analog form by random placement of asterisks in order to mimic photographic grain; the density of asterisks is proportional to the intensity within each resolution element. The Ca^+ K line spectroheliogram, obtained on the same day, shows the close relation between the positions of active regions in the chromosphere, transition zone, and corona.

An important characteristic of the data is the enhancement of active regions, i.e., the ratio of their intensity to that of the quiet sun. Figure 1 shows clearly that the enhancement increases with increasing ionization state, to

the point where, as in Fe XVI, the emission comes almost entirely from active regions.

To investigate this situation quantitatively, we have analyzed the eight individual active regions listed in Table I. For each region, the enhancement was measured in many or all of the spectral lines listed in the table. The first column of the table identifies the line and the second gives T_m, the temperature at which formation of the ion is most strongly favored. Columns 3 - 10 give the number of orbits in which each active region was observed in the various spectral lines. The last column gives the number of observations of the center of the quiet sun used in the analysis for each line. This number is generally less than the total of the active region observations, because often two or more of the active regions were on the visible disk at the same time.

Each spectroheliogram analyzed was the average of five or more individual spectroheliograms made during a single orbit. We defined the intensity of an active region as the average of the four brightest points in an area of enhanced intensity. A few regions were so small that they contained only two or three bright points, in which case those alone were averaged. (There was no apparent correlation between

size of an active region and the enhancement of the line in which it was observed.) We measured only those active regions lying within 0.5 $R_\odot$ of the center, in order to avoid possible effects of limb brightening. We defined the intensity of the quiet sun as the average of the 42 points within a rectangle of dimensions 3 arcmin by 14 arcmin, located at the disk center and oriented with the long axis roughly east-west.

Since subflares in an active region often produced a sudden brightening by a factor of two or more, all spectroheliograms obtained at times when subflares were reported in an active region were deleted from the data for that region. In addition, orbits showing sizeable fluctuations within the region were not used.

The lines O V 758, N IV 765, Ne VIII 770, and O IV 791 lie at wavelengths where there is significant Lyman continuum emission; hence, the observed intensity was due to both the line and the continuum. The intensity due to the continuum alone was measured in a clean window of the spectrum at 800Å. The logarithmic slope d log $I/d\lambda$ of the Lyman continuum has been found (Noyes and Kalkofen, 1969) to be substantially the same in active and quiet regions. Therefore, we were able to use spectral

scans of the quiet sun to deduce the correction factor necessary to scale the intensity of active regions from 800Å to the wavelength of the emission line. The corrected intensity of the Lyman continuum was then subtracted from the observed intensity of the line plus continuum, to give the contribution of the line alone. We applied a similar correction to Si XII 499Å for the underlying helium continuum emission.

For each spectral line and for each active region, all the values for the quiet intensity were averaged and the rms deviation computed. The ratio of the mean value in a given active region to the mean value for all the quiet regions was then computed for each spectral line. Figure 2 shows this ratio for the individual regions, plotted versus log T_m. The error bars denote the extreme values:

$$\frac{A + \Delta A(\text{rms})}{Q - \Delta Q(\text{rms})} \quad , \quad \frac{A - \Delta A(\text{rms})}{Q + \Delta Q(\text{rms})} \quad .$$

The individual active regions were combined and the resulting enhancements plotted in Figure 3. The combined mean shown is the average of the mean values for the individual regions. The rms deviation of the individual means from the combined mean was calculated, and the error bars calculated

in a way similar to those used for the individual regions. The fact that the error bars in Figure 3 are not much larger than those in Figure 2 suggests that the plotted run of enhancement with temperature is a general characteristic of active regions.

The smooth curve superimposed on the data in Figure 3 is the enhancement predicted from a simple model of active regions, which we discuss in the next section. It is also drawn on Figure 2 for reference, and shows that although the general trend is the same for all regions, some individual regions (e.g., McMath Plage #9076) exhibit systematic differences.

3. Discussion

The enhancements shown in Figure 3 enable us to make some interesting comparisons between the structure of active and quiet regions. To reduce the problem to its essentials, we took a simple but successful three-parameter model of the quiet sun (Withbroe, 1969) and applied it to the active region data. The three parameters in the quiet sun model are:

1) The electron pressure P_o at the base of the transition zone between the chromosphere and corona. This is simply a measure of the total mass per cm^2 in the overlying corona.

2) The conductive flux F_c downward from the corona back into the chromosphere. This is assumed to be constant throughout the transition zone, in agreement with findings of Athay (1966) and Dupree and Goldberg (1967). The conductive flux is proportional to the temperature gradient, according to the relation $F_c = \text{const } T^{5/2} \, dT/dh$. Thus F_c measures the sharpness of the temperature rise into the corona..

3) The value of the coronal temperature, T_{cor}. Above the level where the temperature reaches T_{cor}, the corona is assumed to be isothermal.

These three parameters, with the assumptions mentioned, plus the further assumption of hydrostatic equilibrium, completely specify the model for the layers with $T > 10^5$ °K. Below 10^5 °K the temperature gradient no longer varies as $T^{5/2}$ (Athay, 1966) and may be quite complex. There may be a tendency

for temperature plateaus. In addition the simple formula used in calculating the emergent intensities may not be correct for lines with large optical depths formed in the upper chromosphere. For these reasons we have restricted the calculations to the layers with temperatures above 10^5 °K.

The emergent intensities in the normal direction for optically thin lines is given by (Withbroe, 1969):

$$I = \text{const } A \int_0^\infty G(T)\ n_e^2\ dh \qquad (1)$$

where

$$G(T) = \frac{n_i}{n_{el}}\ T^{-5/2}\ 10^{-5040\ W/T}\ , \qquad (2)$$

A is the abundance of the element in question, n_i/n_{el} is the fractional abundance of the ion , and W is the excitation energy in electron volts. We have explicitly assumed that the coronal abundances are the same in both quiet and active areas. The values of n_i/n_{el} used in the calculations include the effects of dielectronic recombination and autoionization processes.

Although the model is a great oversimplification, it does successfully reproduce the spectrum of the quiet sun. The parameters of the quiet sun model are $P_o = 0.10$ dyne/cm^2,

$F_c = 6 \times 10^5$ erg/cm^2/sec, and $T_{cor} = 2 \times 10^6$ °K. Details of the model calculation are described by Withbroe (1969).

In applying this model to active regions, we realize that there is little ground for assuming constant conductive flux or hydrostatic equilibrium in the transition zone. Inhomogeneities in active regions are an additional source of uncertainty for the interpretation of the data. Nevertheless, we retained the three parameters of the model, for they do allow us to vary the mass in the corona, the temperature gradient, and the maximum temperature in the corona in a convenient fashion. Although we are able to fit the data in Figure 3 with such a model, this should not be taken as proof of hydrostatic equilibrium or conductive flux constancy in active regions.

We now ask how the three parameters of the quiet sun model might be changed to produce the contrast shown in Figure 3. For optically thin lines formed in the transition zone and corona (i.e., $T > 10^5$ °K), the emission is proportional to the square of the electron pressure, and thus a simple increase of the electron pressure P_o (leaving the temperature structure unchanged) would cause all the lines for which $T_m > 10^5$ to be enhanced by the same value. It cannot produce

the observed increase of enhancement with T_m, and thus a change in the temperature profile is necessary in addition. In our model we can change the temperature profile either by changing the conductive flux F_c or changing T_{cor}.

A change in the conductive flux chiefly affects lines of ions formed in the transition zone (namely O IV, O V, N IV, N V). Lines of these ions have an emission proportional to $P_o^2 (dT/dh)^{-1}$ (Athay, 1966). Thus increasing F_c or, equivalently, increasing the temperature gradient in the transition zone, causes a proportionate decrease in the intensity of these ions. For ions formed partly in the transition zone and partly in the corona (e.g., O VI, Ne VII, Ne VIII, Mg IX), the decrease is smaller, and pure coronal ions (e.g., Mg X, Si XII, Fe XVI) are unaffected. Figure 4 shows a set of calculations with different values of F_c, leaving P_o and T_{cor} equal to the quiet sun values.

We see that increasing the conductive flux in the transition zone by a factor of about 5 would decrease the enhancement of transition zone lines relative to coronal lines by the observed amount.

The third parameter of the model which we might vary is T_{cor}. An increase in T_{cor} will cause an increase in the

emission from ions for which $T_m > T_{cor}$ and a decrease in emission from ions for which $T_m < T_{cor}$. For ions formed partly in the transition zone, the effect is lessened, and of course it disappears for ions formed purely in the transition zone. Figure 5 shows the results of calculated models in which T_{cor} was varied, leaving P_o equal to the quiet sun value amd F_c equal to five times the quiet sun value.

We see from the figure that the change of enhancement for ions with $T_m < 10^{6.4}$ is small enough to lie within the error bars of our measurements in Figure 3.

Above $T_{cor} = 10^{6.6}$ (i.e., for Fe XV, Fe XVI) the intensity depends very critically on T_{cor}. Unfortunately, the OSO-IV spectrometer was insufficiently sensitive to allow a good determination of the quiet sun intensity in these lines, so that no good value of the enhancement was obtained. However, preliminary results from the recently-launched OSO-VI spectrometer indicate an enhancement of about 50 in Fe XVI. This result is consistent with a slight rise in T_{cor} above quiet sun values, to perhaps 2.5×10^6 °K.

Finally, we are able to determine the pressure increase in active regions by finding the uniform increase in enhancement necessary for an optimum fit between the curves of

Figure 5 and the data of Figure 3, and equating that to the square of the pressure increase. We find the best value of the pressure increase to be about 5. The calculated enhancement for a fivefold increase of both P_o and F_c, and an increase of T_{cor} to 2.5×10^6 °K, is sketched in Figures 2 and 3.

As we mentioned earlier, the fit of the data by our model does not constitute a proof that the conductive flux in active regions is proportional to $T^{5/2}$ dT/dh. However, let us examine the situation if this actually were the case. Then the increased temperature gradient above active regions would imply an increase of flux conducted down into the chromosphere. Therefore, we would require that the mechanical energy deposited in the corona above active regions be increased by the same amount, if the main source of energy loss from the low corona is thermal conduction downward, as it is in the quiet sun (Kopp, 1968). A fivefold increase of conductive flux downward also would imply a fivefold increase in the energy emitted from the top of the chromosphere. This could be in the form of either radiation or mechanical energy transport (see e.g., Kuperus and Athay, 1967). It is suggestive that the enhancement seen in the hydrogen and helium lines and continua, which are the main radiators in the upper chromosphere is about a factor of five (Figure 3).

Although the simple model described above can explain the general trend of enhancements for $T_m > 10^{5.4}$ and can make plausible the enhancements seen in the chromosphere ($T_m < 10^5$), it fails completely to explain the rather pronounced minimum of enhancement seen in Figure 3 for $10^{5.0} < T_m < 10^{5.4}$. However, we suspect that this minimum is not attributable to the density or temperature structure of active regions, but rather to overlying Lyman continuum absorption. By coincidence, the lines of those ions which lie in the temperature range $10^{5.0} < T_m < 10^{5.4}$ (namely O II 718, O III 702, N IV 765, O IV 789, O V 758, and O V 630) all lie within the Lyman continuum. Although, as we stated in Section 2, the emission of nearby continuum was subtracted out from those lines for which it was important, it is possible that in active regions the line emission itself is diminished by Lyman continuum absorption due to overlying cool material. From recent OSO-VI observations, we have found that of the two resonance lines N III 991 and N III 685 Å, which lie on either side of the Lyman limit, the former has an enhancement about 1.5 times that of the latter. This result suggests that the minimum is indeed due to the existence of the Lyman continuum. If this is the case, it implies that the chromosphere in active regions is so inhomogeneous that significant amounts of cool gas exist above

material at a temperature of 10^5 °K. Some or all of the cool gas might be in the form of prominences overlying the active regions.

To summarize, we conclude that in a typical active region, the pressure is increased about a factor of five over the quiet sun value, the temperature gradient is increased a similar amount, and the coronal temperature is increased slightly, to about 2.5×10^6 °K. Chromospheric lines are enhanced about a factor of five, and may reflect a fivefold increase of mechanical energy deposited in the low corona and conducted back down to the chromosphere.

The value of the increases should be interpreted as representative only, and may well vary considerably among different active regions. Certainly such variation is one source of the uncertainty in the data plotted in Figure 3. Unfortunately the OSO-IV data are not extensive enough to permit detailed analysis of individual regions. However, new data recently acquired by the Harvard spectrometer aboard the OSO-VI spacecraft should soon provide a much more complete description of the structure of individual active regions in the chromosphere and corona.

ACKNOWLEDGEMENTS

We wish to thank Professor Leo Goldberg, Dr. E.M. Reeves, Dr. W.H. Parkinson, and other members of the Harvard Solar Satellite project for successfully undertaking the enormous challenge of designing, producing, and operating the HCO OSO-IV Spectrometer. We are indebted to Mrs. Judith Flagg and Mrs. Jennifer Garg for programming assistance. This work is supported by the National Aeronautics and Space Administration through contract NASw-184.

REFERENCES

1. ATHAY, R.G.: 1966, 'Theoretical Line Intensities. V. Solar UV Emission Lines of Heavy Elements,' Ap. J. 145, 784.

2. DUPREE, A.K. and GOLDBERG, L.: 1967, 'Solar Abundance Determination from Ultraviolet Emission Lines,' Solar Physics 1, 229.

3. GOLDBERG, L., NOYES R.W., PARKINSON, W.H., REEVES, E.M., and WITHBROE, G.L.: 1968, 'Ultraviolet Solar Images from Space,' Science 162, 95.

4. KOPP, R.A.: 1968, 'The Equilibrium Structure of a Shock-heated Corona,' Thesis, Harvard University, Cambridge, Massachusetts, U.S.A.

5. KUPERUS, M. and ATHAY, R.G.: 1967, 'On the Origin of Spicules in the Chromosphere-corona Transition Region,' Solar Phys., 1, 361.

6. NEWKIRK, G., Jr.: 1967, 'Structure of the Solar Corona,' Ann. Rev. Astron. & Astrophys. 5, 213.

7. NOYES, R.W. and KALKOFEN, W.: 1969, 'Observations and Interpretation of the Solar Lyman Continuum,' to be submitted to Solar Physics.

8. ROGERSON, J.B., Jr.: 1961, 'On Photospheric Faculae,' Ap. J. 134, 331.

9. SHEELEY, R.R.: 1967, 'The Average Profile of the Solar K-Line During the Sunspot Cycle,' Ap. J. 147, 1106.

10. WITHBROE, G.L.: 1969, 'XUV Limb-brightening Observations I: The Lithium-like Ions,' Solar Physics, in press.

TABLE 1

Details of Active Region Observations

Spectral Line	log T_m	Number of Orbits Observed in Mc Math Region No. 9049	9048	9082	9089	9091	9088	9076	9067	Total Quiet Orbits
Ly Cont. 800	4.0	1	1	3				1	4	9
O I 1305	4.3	3	3							3
He I Cont. 504	4.5	2	2							4
He I 584	4.5	2	2							4
C II 1335	4.6	3	3						1	6
N II 1085	4.7	3	2							4
O II 718	4.8	2	2							2
C III 977	4.9	1	1							2
C III 1176	4.9	1	1							1
He II 304	4.9	4	4							5
N III 991	5.0			5	4	3	4	1	1	8
O III 702	5.0	3	3							3
N IV 765	5.2	1	1							1
O IV 554	5.2	2	2							3
O IV 791	5.2	4	3	3	4	3	4	1	1	12
O V 630	5.4	3	2							3
O V 758	5.4	1	1							1
O VI 1032	5.5	3	3	6	5	4	4	3	4	17
Ne VII 465	5.8	1	1							1
Ne VIII 770	5.9	3	3	3	6	4	6	1	2	12
Mg IX 368	6.1	2	2							2
Mg X 625	6.2			4	7	6	7	20	9	32
Si XII 499	6.4	6	6	4	7	6	6		3	17

FIGURE CAPTIONS

Figure 1. Sequence of EUV spectroheliograms obtained by the HCO spectroheliometer aboard OSO-IV on November 26, 1967. The four active regions closest to the disk center were used in the analysis. Their McMath Plage Numbers are: (upper left) 9089, (upper right) 9082, (lower center) 9091, and (lower left) 9088. The Ca II 3933 spectroheliogram is courtesy of McMath-Hulbert Observatory.

Figure 2. Enhancement of the individual active regions listed in Table 1. For description of error bars, see text. Solid line is the prediction of the model described in Section III.

Figure 3. Mean enhancement of the active regions listed in Table 1. For description of error bars, see text. Solid line is the prediction of the model described in Section III.

Figure 4. Calculated enhancement I_A/I_Q for various values of the ratio of conductive flux F_c in active regions to that in the quiet sun. The chromospheric electron pressure P_o and the coronal temperature T_{cor} are left equal to the quiet sun values. The dashed curve is the adopted ratio $F_c\ (A)/F_c(Q) = 5$.

Figure 5. Calculated enhancement I_A/I_Q for various values of the coronal temperature T_{cor} in active regions. The conductive flux ratio $F_c(A)/F_c(Q)$ is set equal to 5 (as the dashed curve in Figure 4) and the chromospheric electron pressure P_o is left equal to the quiet sun value.

OSO-IV SPECTROHELIOGRAMS - Nov 26, 1967

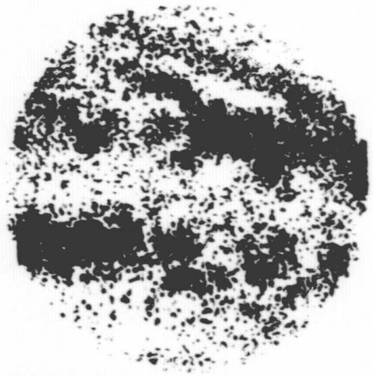

Ly Cont 800

N III 991

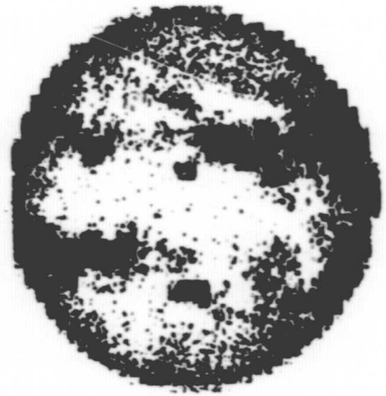

O VI 1032

Ne VIII 770

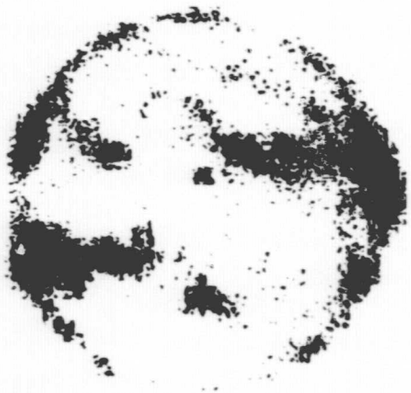

Mg X 625

Si XII 499

Fe XVI 361

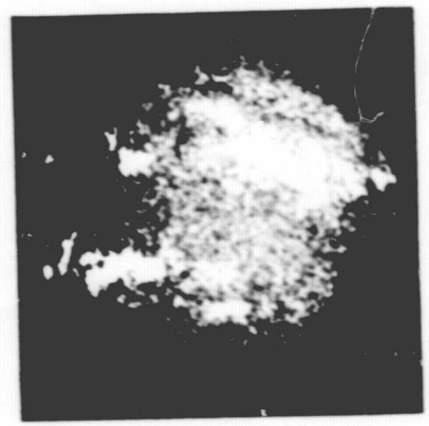

Ca II 3933

Figure 2

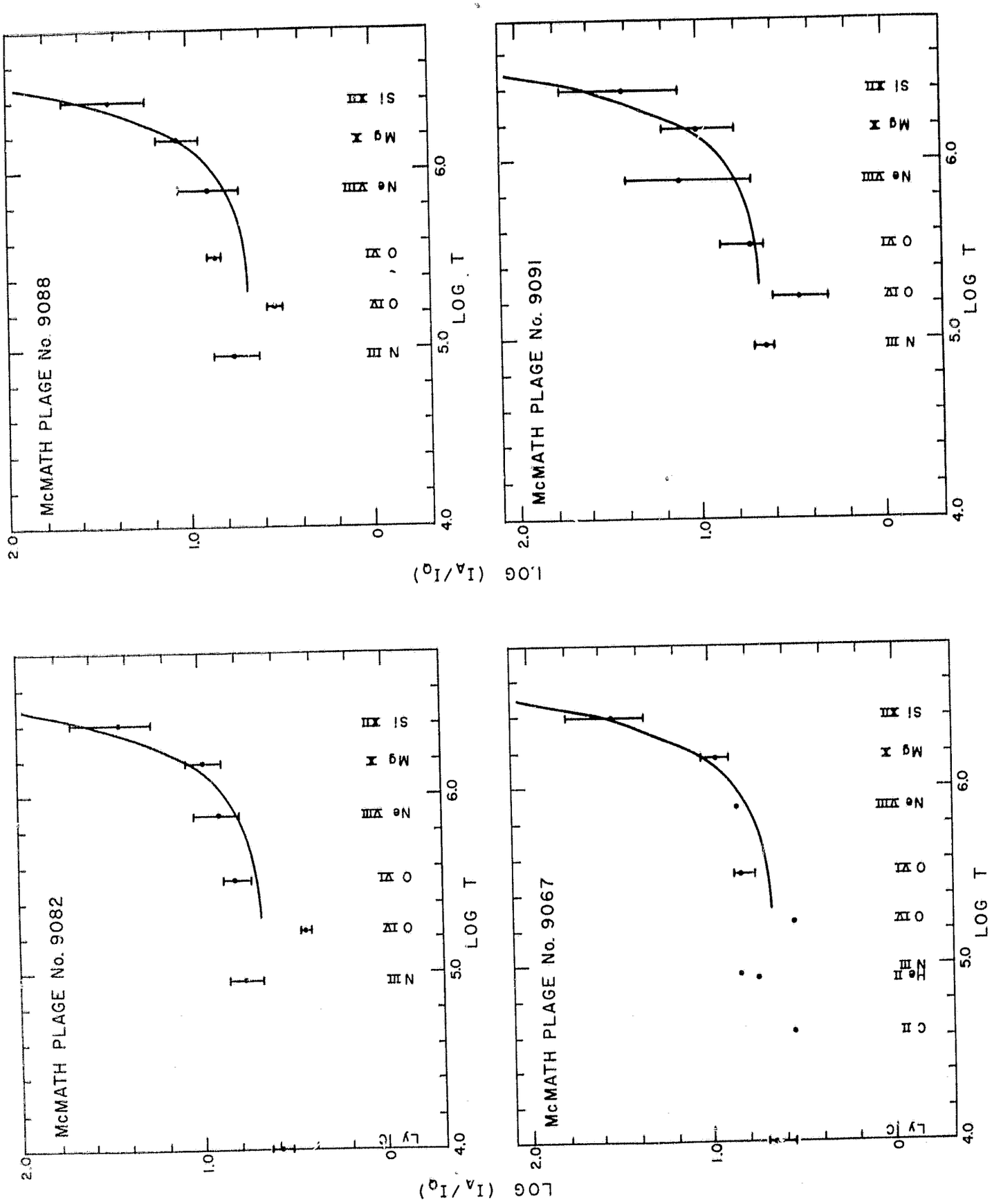
McMATH PLAGE No. 9088
McMATH PLAGE No. 9091
McMATH PLAGE No. 9082
McMATH PLAGE No. 9067
LOG (I_A/I_Q)
LOG T
Si XII
Mg X
Ne VIII
O VI
O IV
N III
Ly ζ
He II
C II
2.0
1.0
0
4.0
5.0
6.0

Figure 2
(continued)

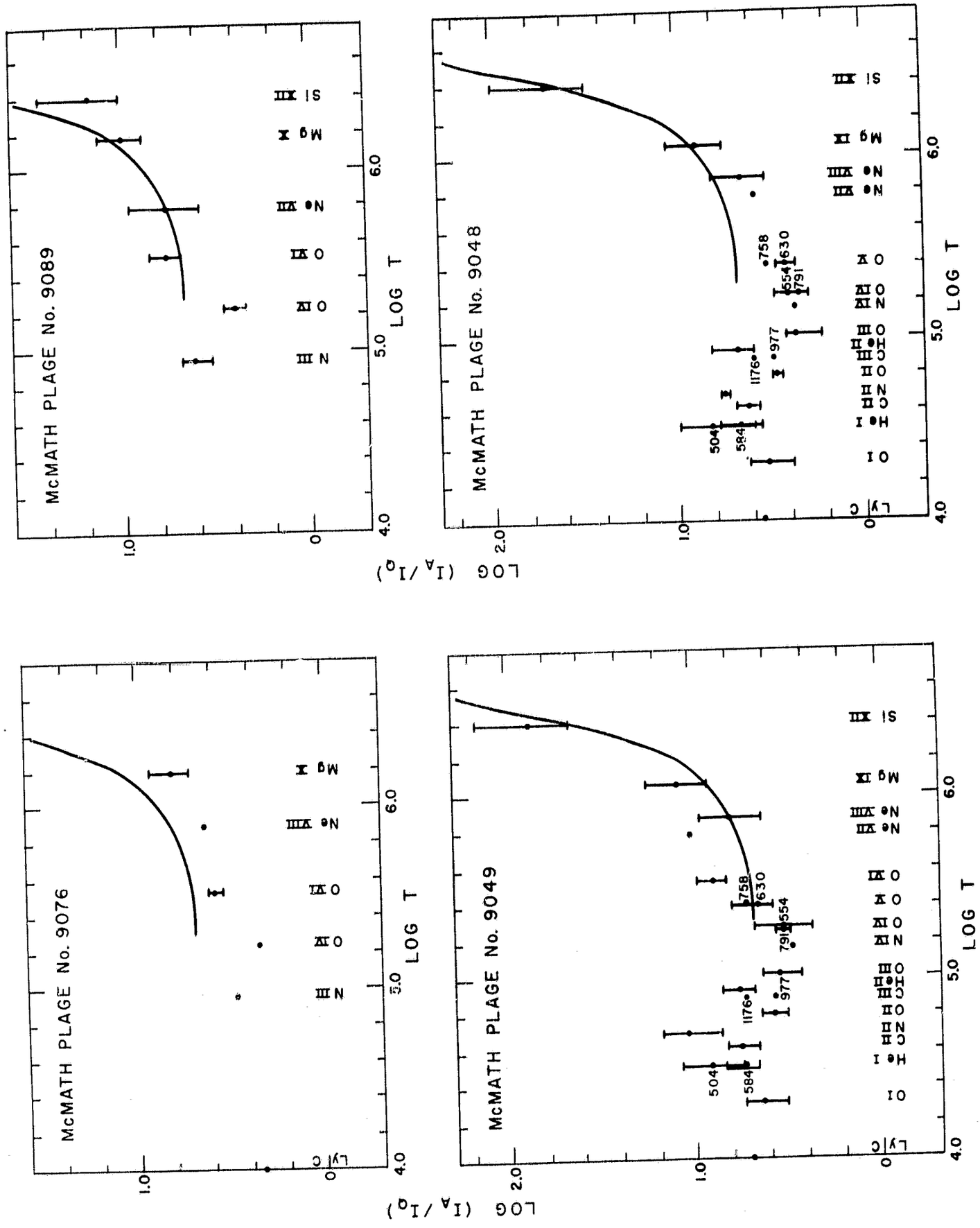

Figure 3

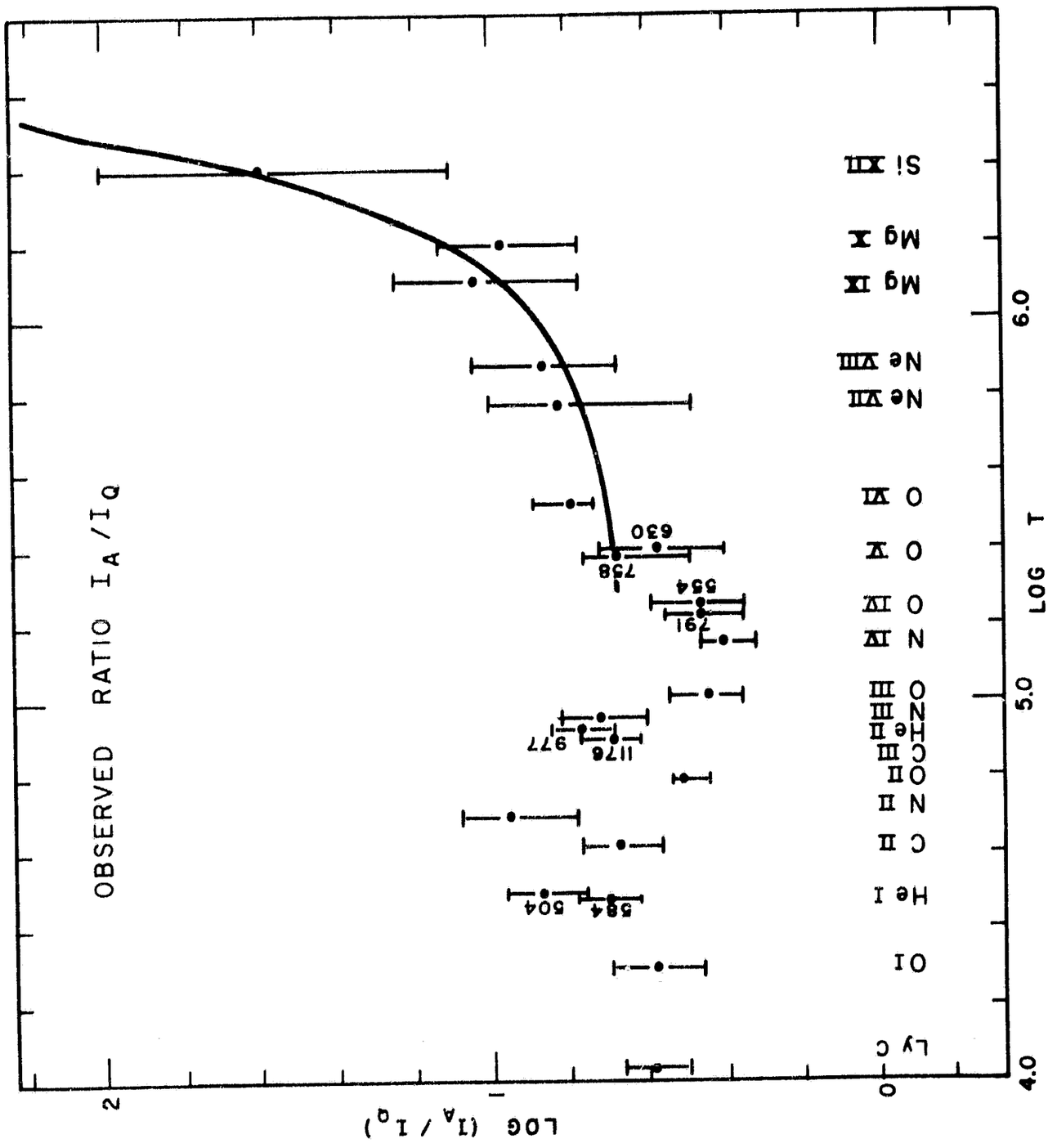
OBSERVED RATIO I_A / I_Q
LOG (I_A / I_Q)
LOG T
2
0
-
4.0
5.0
6.0
Ly C
O I
He I
C II
N II
O II
C III
He II
N III
O III
N IV
O IV
O V
O VI
Ne VII
Ne VIII
Mg IX
Mg X
Si XII
584
504
1176
977
791
554
738
630

Figure 4

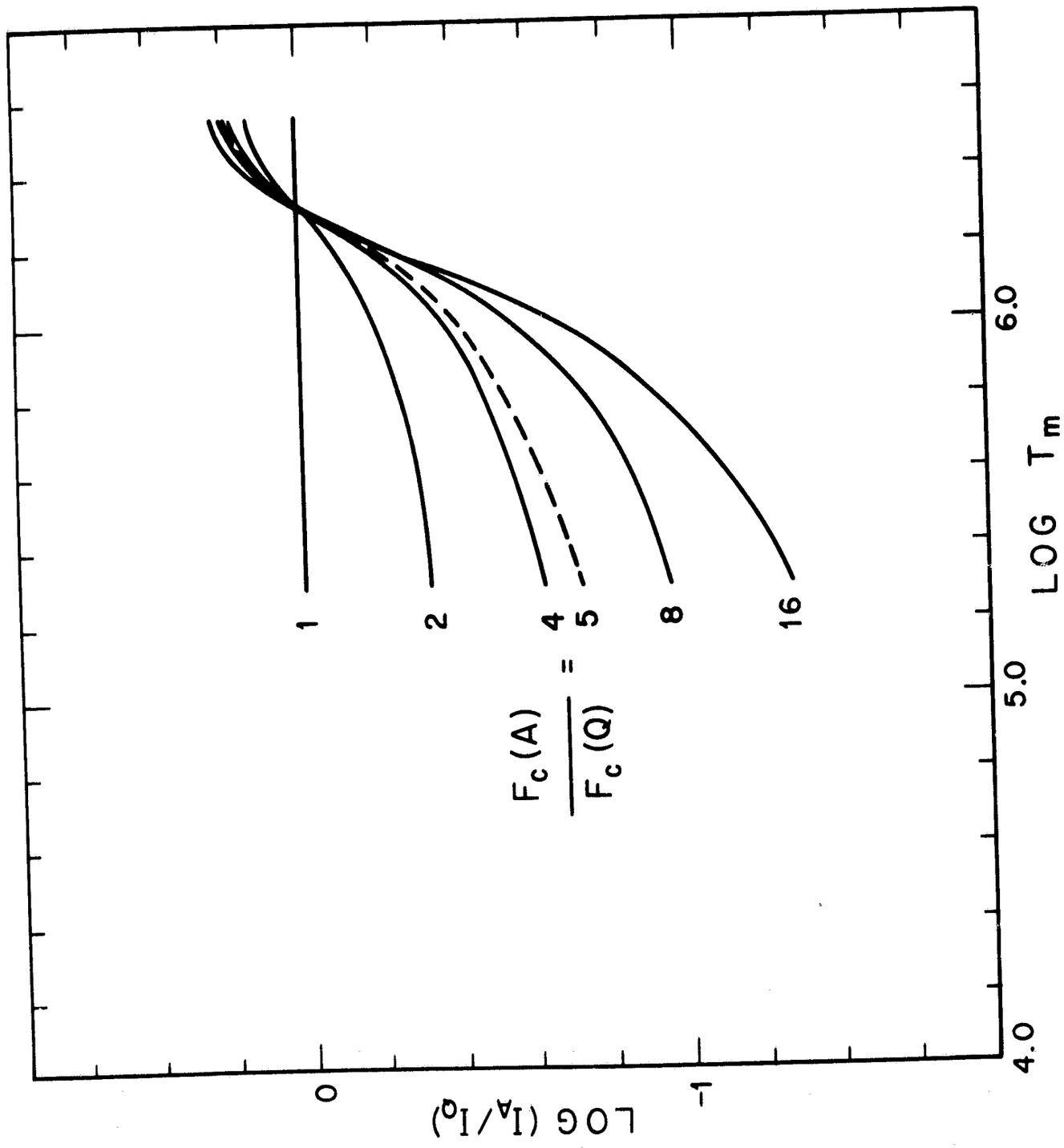

Figure 5